



### **Science Arts & Métiers (SAM)**

is an open access repository that collects the work of Arts et Métiers Institute of Technology researchers and makes it freely available over the web where possible.

This is an author-deposited version published in: <https://sam.ensam.eu>  
Handle ID: <http://hdl.handle.net/10985/18121>

#### **To cite this version :**

Michal LIPIAN, Ivan DOBREV, Maciej KARCZEWSKI, Fawaz MASSOUH, Krzysztof JOZWIK - Small wind turbine augmentation: Experimental investigations of shrouded- and twin-rotor wind turbine systems - Energy - Vol. 186, p.115855 - 2019

Any correspondence concerning this service should be sent to the repository

Administrator : [scienceouverte@ensam.eu](mailto:scienceouverte@ensam.eu)



# Small wind turbine augmentation: Experimental investigations of shrouded- and twin-rotor wind turbine systems

Michał Lipian <sup>a,\*</sup>, Ivan Dobrev <sup>b</sup>, Maciej Karczewski <sup>a</sup>, Fawaz Massouh <sup>b</sup>, Krzysztof Jozwik <sup>a</sup>

<sup>a</sup> Institute of Turbomachinery, Lodz University of Technology, 219/223 Wolczanska Street, 90-924, Lodz, Poland

<sup>b</sup> Laboratoire DynFluid, Arts et Métiers ParisTech, 151 Boulevard de l'Hôpital, 75013, Paris, France

---

## A B S T R A C T

An increase in the efficiency of Small Wind Turbines (SWTs) by aerodynamic optimisation of the blade geometry is limited (low Reynolds number influence). Solutions such as the Diffuser-Augmented Wind Turbine (DAWT) and the twin-rotor systems are of increasing interest. A diffuser promotes an increase in the wind mass flow rate through the turbine, whereas an auxiliary rotor enables extraction of the wind kinetic energy in the wake.

The paper summarizes the measurements of wind turbine systems performance conducted at the Institute of Turbomachinery, Lodz University of Technology (IMP TUL). The research incorporated a spectrum of wind turbine configurations for open and shrouded, single- and twin-rotor systems. The objective was to compare the performance of the same rotor in different configurations. The influence of a low Reynolds number flow on the rotor performance is also discussed and quantified.

The study shows that, while augmenting the wind turbine performance (as much as twofold increase), shrouding rises significantly the rotor loading. A remedy for that may be an application of the second rotor. Although it provides a rather modest efficiency increase (11–13% for the unshrouded-, 4–5% for shrouded turbine), it allows loads to be distributed more evenly on turbines.

---

## 1. Introduction

Although the concept of a stator-equipped wind turbine was studied back at the beginning of the 20th century, the first practically feasible solutions were presented around the 1980s. Igra [1] was studying diffusers of a long form, inspired by turbomachines. Gilbert and Foreman [2] proposed a design based on an aerodynamic profile. The drawback of those early solutions was their large size and mass – thus, also the cost. There was little practical interest in this idea, due to its financial inefficiency. The concept remained unexplored until the addition of a flange (or a brim) at the diffuser exit, as proposed by Abe and Ohya [3]. Modern economic studies (e.g., Ref. [4]) show the purposefulness of shrouded wind turbines, as standalone or hybrid installations. It is important to underline that most of these machines are of small scale and power up to about 50 kW, falling into the definition of a Small Wind Turbine [5]. The authors of this article believe that distributed installations and local ownership of wind turbines will develop

further in the years to come, although these actions must be supported by the interested parties [6].

### 1.1. Experimental investigations in shrouded- and twin-rotor wind turbines

The majority of the earliest research pertaining to the DAWT was related to experimental investigations. Igra [1] performed a profound analysis of various shroud geometries, both in the wind tunnel and in field tests (a prototype of the rotor diameter  $D = 3$  m and the power  $P = 0.66$  kW at 5 m/s was constructed). Gilbert and Foreman [2] conducted a series of wind tunnel experiments for different rotor loadings and sizes (the maximal diameter equal to 0.46 m). Nagai validated his analytical research [7] using the results from earlier prototype measurements, although no precise technical specification was made available. More recently, diffusers were shortened into a more compact form and equipped with an exit flange. This enlarged the underpressure region downstream of the shroud and further increased the mass flow through the diffuser. Kosasih and Tondelli [8] observed how their model wind turbine of  $D \approx 0.2$  m performed with different shapes of the

---

\* Corresponding author.

E-mail address: [michal.lipian@p.lodz.pl](mailto:michal.lipian@p.lodz.pl) (M. Lipian).

## Nomenclature

ABS	Acrylonitrile butadiene styrene
CROR	Counter-Rotating Open Rotor
CRSR	Counter-Rotating Shrouded Rotor
DAWT	Diffuser-Augmented Wind Turbine
FFT	Fast Fourier Transform
IMP	Institute of Turbomachinery
SWT	Small Wind Turbine
TUL	Lodz University of Technology
$A, m^2$	Rotor area
$C_p, -$	Power coefficient
$C_t, -$	Thrust coefficient
$D, m$	Diameter
$F_t, N$	Rotor thrust (axial force)
$P, W$	Power

$Q, N \cdot m$	Rotational torque
$Re, -$	Reynolds number
$RH, -$	Relative humidity
$T, K$	Temperature
$TSR, -$	Tip speed ratio (also $\lambda$ )
$V, m/s$	Wind velocity
$c, m$	Chord length
$l, m$	Characteristic length
$p, Pa$	Pressure
$p_{abs}, Pa$	Ambient pressure
$p_{dyn}, Pa$	Dynamic pressure
$r, J/kg \cdot K$	Individual gas constant
$v, m/s$	Velocity
$\nu, m^2 \cdot s$	Kinematic viscosity
$\rho, kg/m^3$	Density
$\omega, rad/s$	Rotational velocity

diffuser and with an application of an inlet nozzle in order to increase wind turbine performance. Abe et al. [9] used hot wire anemometry to reconstruct the velocity field around the open- and shrouded wind turbine. The flow directly downstream of the blades was similar in both cases, with only minor differences in the tip region. In return, strong dissimilarities were observed further on, with a rapid destruction of the vortex wake in the case of the DAWT, credited to a damping effect of the diffuser. Wang et al. [10] used wind tunnel tests to assess the mechanical behaviour of a shrouded rotor of the 3 kW wind turbine. In telemeter tests, it was possible to determine stresses in the blades operating at different wind speeds and yawing angles, and to conclude that an addition of shrouding increases the said stresses. The DAWT concept also resonates in vertical-axis wind turbines, where the shroud usually has a form of vanes directing the flow similarly as in case of classic two-stage turbines (see, e.g., Ref. [11]). The investigations performed at the IMP TUL included tests in a low-speed wind tunnel [12]. The experiment involved PIV flow imaging of an empty diffuser, pneumatic measurements and determination of the wind turbine model power.

Wind turbine power is proportional to the rotor area  $A$  (see Eq. (1)), which can be increased by elongating the blades or adding the second rotor. An advantage of the latter solution is a more even distribution of stresses between multiple stages of the turbine, as stated by Curtis in his patent of an impulse turbine [13]. A significant obstacle in optimising a multi-rotor wind turbine system remains the wake phenomena, since most studies are oriented towards wind farm optimisation and far wake exploration [14]. Due to a lack of nozzle blades, twin-rotor wind turbines are usually Counter-Rotating Open Rotor (CROR) devices. Appa [15] proposed a CROR wind turbine composed of two rotors of the same geometry ( $D = 4$  m). The prototype installation managed to increase the system aerodynamic efficiency by 25–40% (compared to the single rotor), and this gain was most visible for low rotational velocities. Jung et al. [16] proposed to place a smaller, auxiliary rotor upstream of the main rotor, resulting in a 30 kW-CROR of the total efficiency around 50%. Several studies proposed a CROR in which the upstream rotor diameter was bigger than that of the downstream one [17–19]. The wind tunnel measurements permitted optimisation of the entire system by a proper choice of the number and size of blades, types of aerofoils, chord and twist angles, etc. The wind turbines were designed to work with a custom-made generator, in which both armatures were rotating. Field tests were also

performed, with promising results, yielding 430 W at 12.6 m/s ( $D_{upstream} = 2$  m,  $D_{downstream} = 1.33$  m).

A combination of the DAWT and CROR concepts seems a natural idea, as it would enable one to profit further on from the diffuser-enhanced wind velocity by placing the second rotor in the augmented velocity region. An example of a (failed) attempt at this concept was the so-called Elena Energie wind turbine (see, for instance, Ref. [20]) installed and tested in Paris Belleville park. No scientific data concerning its geometry or performance was shared. A different approach, a multi-DAWT array, was explored by Göltenbott [21]. An interaction between neighbouring shrouded wind turbines was examined in a wind tunnel. It was reported that the array could obtain higher power than individual DAWTs, which was attributed to the flow acceleration between neighbouring wind turbines, measured with hot-wire anemometry.

The current study proposes a novel approach to the investigation of DAWTs and CRORs, as the rotors studied for all the cases have the same geometry. Thus, the results can be easily compared. The machine being their combination, the CRSR (Counter-Rotating Shrouded Rotor), is examined profoundly to determine a possibility of its employment in modern wind turbine systems. The objective was therefore to compare the performance of the very same rotor at different configurations by using experimental analysis in the wind tunnel. The quantification of a low Reynolds number flow influence on the rotor performance is another important aspect under discussion. In total, 9 cases were examined, as shown in Table 1.

## 1.2. Definition of the dimensionless variables

The shrouded wind turbine operates at the local wind velocity higher than that of an open rotor. This enables it to attain relatively higher power values at the same reference wind speed, compared to an open rotor. Even a small change in the wind velocity  $V$  exerts a significant effect on the power outcome  $P$  and the thrust force  $F_t$ , as they are expressed as (see, e.g., Ref. [22]):

**Table 1**  
Overview of the analysed cases.

	Open rotor	DAWT	CROR	CRSR
No. of rotors	1	1	2	2
Diffuser	no	yes	no	yes
No. of locations	1	2	3	3

$$P = P_{wind} C_p = \frac{\rho A V^3}{2} C_p \quad (1)$$

$$F_t = F_{twind} C_t = \frac{\rho A V^2}{2} C_t$$

In the above formulae,  $P_{wind}$  and  $F_{twind}$  denote, respectively, the power and axial force of an air stream of the same cross-section area as the rotor.  $\rho$  denotes fluid density.  $C_t$  is referred to as the thrust coefficient, whereas  $C_p$  is the so-called power coefficient, which can be understood as rotor efficiency. It can be demonstrated (see ex. [23]) that the maximal  $C_p$  for an open rotor is attained when the wind velocity in the wake becomes 1/3 of the reference velocity  $V$ . Then:

$$C_{pmax} = \frac{16}{27} \approx 0.593 \quad (2)$$

The above formula defines the so-called Betz limit, the maximal open rotor efficiency. The situation changes, however, when shrouding is applied, as it modifies locally velocity and pressure fields (e.g., Nagai [7]). Similarly, when considering a twin-rotor system (e.g., Newman [24]), it is possible to demonstrate that the maximal total  $C_p$  is equal to 0.64, that is 8% more than for a single rotor wind turbine (assuming the same rotor area for both wind turbines).

In order to compare the performance of wind turbines operating at different flow conditions, it is also necessary to recall the Reynolds number  $Re$  definition:

$$Re = \frac{v l}{\nu} \quad (3)$$

In the above equation,  $v$  is the velocity (local wind speed in the current study),  $l$  is the characteristic length (equal to the chord length  $c$  in this case) and  $\nu$  is the kinematic viscosity.

In order to assess an influence of the wind turbine rotational velocity  $\omega$ , the so-called tip-speed ratio TSR is defined as:

$$TSR = \frac{\omega D}{2V} \quad (4)$$

Note that in (4),  $\omega$  is placed in [rad/s] in order to represent the linear velocity of the blade tip. Thus, in theory the above formula should be multiplied by [1/rad] to obtain the TSR as a dimensionless parameter. This is usually omitted, since radian is an SI dimensionless unit (see, e.g., Ref. [22]).

## 2. Experimental apparatus

Experimental investigations of SWTs constitute a significant challenge due to numerous aspects. As observed by Sætran (e.g., Ref. [25]), the low-local Reynolds number flow around aerofoil causes boundary layer transition and separation to be much more unpredictable and dependent on external factors, such as turbulence intensity. Additionally, as tested models become smaller, the surface quality becomes an important factor to be considered. Roughness is an important issue [26] in certain 3D-printing technologies, as layers of materials are placed on one another, resulting in a non-smooth surface.

### 2.1. Methodology

The measurement system (Fig. 1) involves devices used to evaluate flow properties (ambient pressure  $p_{atm}$ , temperature  $T$ , relative humidity  $RH$ , dynamic pressure  $p_{dyn}$ ) used to estimate the flow velocity  $V$  and perform temperature compensation;

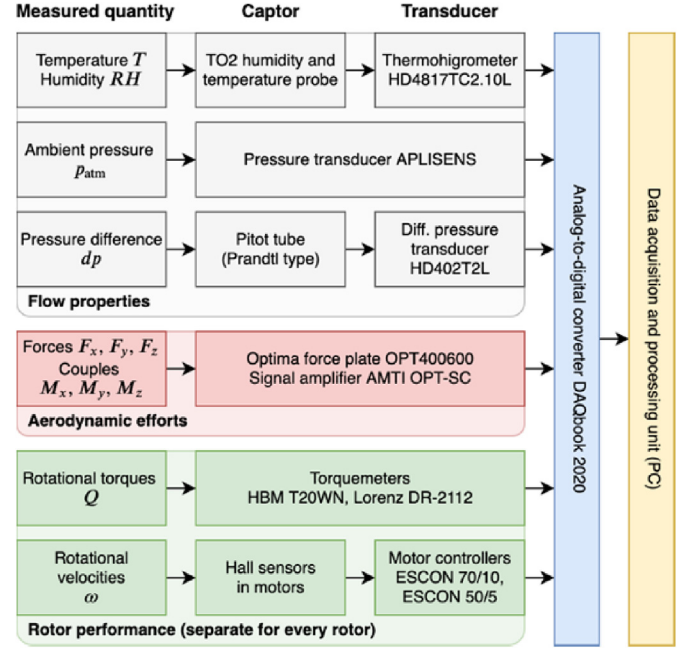


Fig. 1. Wind turbine experimental measurement system; colours distinguish main elements of the measurement chain; first three columns show measured quantities, captors and transducers used, respectively.

aerodynamic forces (the rotor thrust or the axial force  $F_t$ ); and rotor performance (the rotational torque  $Q$  and the angular velocity  $\omega$ ).

The flow velocity  $V$  is evaluated on the basis of pneumatic measurements with a Pitot tube (Prandtl type). The obtained (dynamic) pressure is recomputed into the wind velocity  $V$  as [27]:

$$V = \sqrt{\frac{2 dp}{\rho}} \quad (5)$$

To account for changes in flow thermodynamic conditions in the wind tunnel, the density  $\rho$  is calculated separately for every test point [27]. Humid air is treated as a mixture of two ideal gases: dry air and water vapour. The flow medium density is a sum of densities of both constituting ideal gases:

$$\rho = \rho_{dry} + \rho_{vap} = \frac{p_{dry}}{r_{dry} T} + \frac{p_{vap}}{r_{vap} T} \quad (6)$$

$$p_{dry} = p_{atm} - p_{vap} \quad (6a)$$

$$p_{vap} = RH p_p \quad (6b)$$

In formula (6),  $r_{dry} = 287.05 \text{ J/kg} \cdot \text{K}$  and  $r_{vap} = 461.50 \text{ J/kg} \cdot \text{K}$  are individual gas constants for dry air and water vapour, respectively.  $p_{dry}$  and  $p_{vap}$  are the partial pressures of dry air and water vapour, correspondingly. The former is computed basing on the Dalton's law (6a), the latter – the relative humidity  $RH$  and the saturation vapour pressure  $p_p$  (6b).  $p_p$  can be computed with empirical formulae. In this case, the so-called Buck equation [28] was used (with temperature expressed in  $^{\circ}\text{C}$ ):

$$p_p = 611.21 \exp\left(\left(18.678 - \frac{T}{234.5}\right) \left(\frac{T}{257.14 + T}\right)\right) \quad (7)$$

Wind turbine performance was determined by measuring the shaft angular velocity  $\omega$  and the torque  $Q$ . The product of both the quantities is the rotor power:

$$P = Q \omega \quad (8)$$

Before the measurement campaign, the idle test setup torque (coming from friction, bearings, etc.) was determined. For this purpose, the rotor was detached and torque was measured at different rotational velocities. Similarly, the rotor thrust measurements were preceded by test platform drag evaluation. Those steps enabled to compensate the obtained results for local losses.

The measurement acquisition rate was equal to 1000 Hz, with 65536 samples collected. This enabled a rudimentary signal analysis with the Fast Fourier Transform (FFT) and creation of a simple 2nd order band reject Butterworth filter, targeting the dominant signal frequencies (coming from, e.g., a wind tunnel ventilator and the wind turbine rotational velocity).

Standard procedures were used in order to assess the measurement uncertainty. The assessment took into account the statistical evaluation of the collected data (type A uncertainty) and the

accuracy of the measuring equipment/system (type B uncertainty). The combined standard uncertainty for TSR,  $C_p$  and  $C_t$  for single rotor cases are represented in Figs. 6 and 7 as error bars for all measurement points. The relative uncertainty is especially high for  $C_t$  at low wind speeds (e.g., 7.7 m/s and 10.0 m/s in Fig. 6), which proves that the results in these cases may be biased and must be considered mostly for qualitative analysis. For twin-rotor configurations, the uncertainties are not presented in the graphs so as to not obscure them. In these cases, the order of magnitude of relative combined standard uncertainty for TSR values is 1%,  $C_p$ : 2%,  $C_t$ : 3–4%.

## 2.2. Wind turbine test platform

The IMP TUL subsonic wind tunnel [29] has an open test section operating in the blow mode. Air is moved by a centrifugal fan of the nominal volume flow rate equal to 6.25 m<sup>3</sup>/s. An installation of

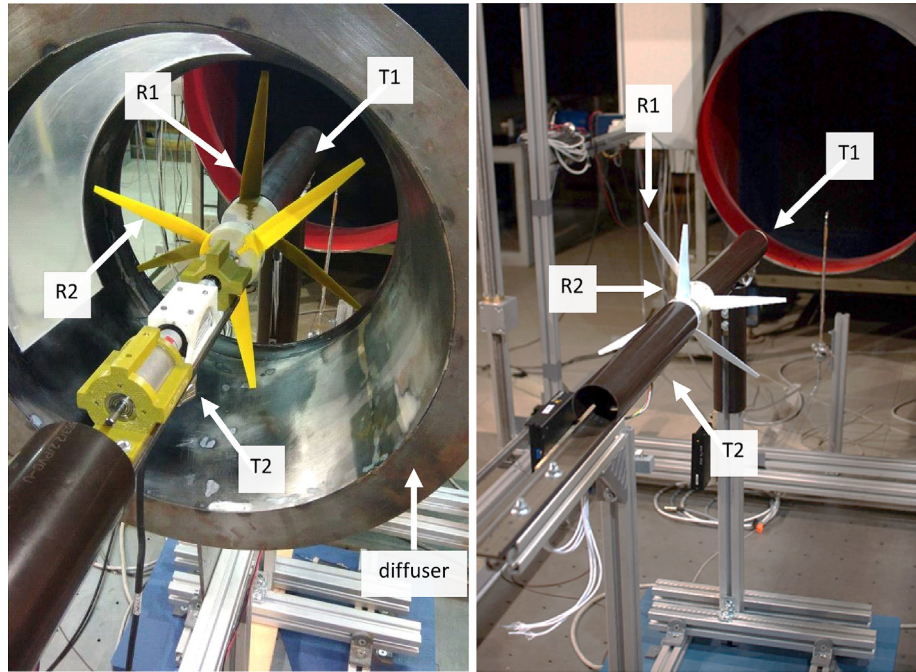


Fig. 2. Various components of the test platform: rotors (R1 downwind, R2 upwind), test setups (T1 upstream, T2 downstream), diffuser.

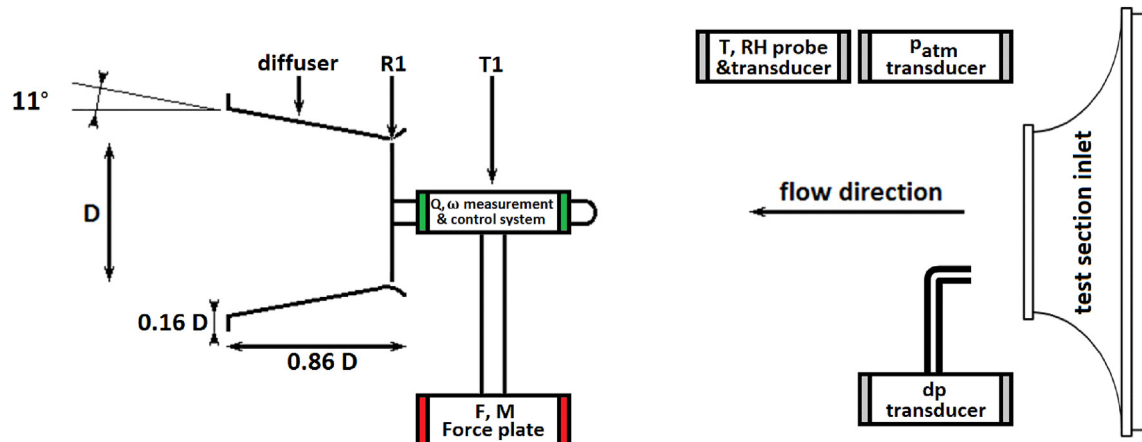


Fig. 3. Schematic view of the complete test platform in the DAWT measurements (elements not in scale).





Fig. 4. 3D printed blades view: top, pressure side, leading edge side.

honeycomb [30] and recent renovation works adapted the wind tunnel structure for current aerodynamic projects conducted at the IMP TUL. The wind tunnel outlet (test section inlet) is of circular shape. The test section has the diameter of 0.8 m and the length of 2 m. The maximal achievable air velocity is equal to approximately 18 m/s.

The test platform consists of three principal elements (Figs. 2 and 3):

- T1 upstream wind turbine – the default wind turbine used for the tests, placed closer to the test section inlet, at the default distance of 1 m from it,
- T2 downstream wind turbine – the second wind turbine, whose streamwise position with respect to T1 can be adjusted,
- Diffuser – a divergent duct; wind turbines are placed at its inlet and inside.

Both the three-bladed rotors under consideration share the same geometry, based on SG6040 and SG6041 aerofoils. The blade geometry of a spanwise-variable chord and a twist angle (Fig. 4, see Ref. [31]) is an in-house IMP TUL design for a DAWT. The rotor diameter  $D$  is equal to 0.32 m. This value was chosen in previous analyses conducted at the IMP TUL [32] as a compromise between small scale and wind tunnel blockage. At the wind velocity of 15.95 m/s and the optimum TSR, the local Reynolds number calculated on the basis of the chord length is of the order of magnitude equal to  $10^5$ . The diffuser is a divergent duct of cut-cone shape of the total length of approximately  $0.86 D$ , cone angle of  $22^\circ$  and the tip clearance around  $2.2\% D$  (Fig. 3). The diffuser inlet is equipped with a convergent section (“throat”). It attracts more mass flow through the diffuser inside and tranquilizes the flow to

prevent additional separations. The diffuser outlet is equipped with a brim, installed to increase the low-pressure zone downstream of the diffuser and, additionally, to increase the mass flow rate through the rotor.

Each wind turbine is controlled and measured separately, on a test setup composed of four principal components (Fig. 5), namely:

- Rotor – composed of three blades, fixed to the hub. The blades and the hub are 3D-printed (Fused Deposition Modelling technique), using acrylonitrile butadiene styrene (ABS) as the material, and surface-treated to decrease roughness (see Ref. [33] for more details on the process). This ensures high fidelity of depiction of the designed geometry. Two rotor specimens are used, R1 and R2, the latter being a mirrored geometry of the former one.
- Bearing unit – supporting the rotor shaft. Three straight ball bearings constitute an over rigid arrangement to minimize the vibrations coming from the rotor and to increase robustness.
- Torquemeter – captor-transducer used to measure the torque produced by the wind turbine rotor and transported via the shaft.
- Permanent magnet motor/generator – used to impose actively the system rotational velocity. The device itself is regulated by a dedicated four-quadrant controller working in a closed loop, maintaining the rotational velocity. It also governs if the energy transformer works in the motor mode (propelling the rotor) or the generator mode (converting mechanical energy into electricity). A connection of the electric circuit to the battery accumulator enables electric energy supply and storage in the same source.

All the aforementioned components are housed in tailor-made holders, manufactured in 3D printing technology. This process ensures rapidity and gives virtually unlimited possibilities of adapting the holders' shapes. All elements are mounted on a C-profile, which in turn is mounted on a pillar. The test setup and the pillar are enclosed in covers made of a plastic pipe, to decrease their aerodynamic drag.

### 3. Results and discussion

The measurement campaign consisted of several steps: investigations of the SWT behaviour at low wind speeds, results of

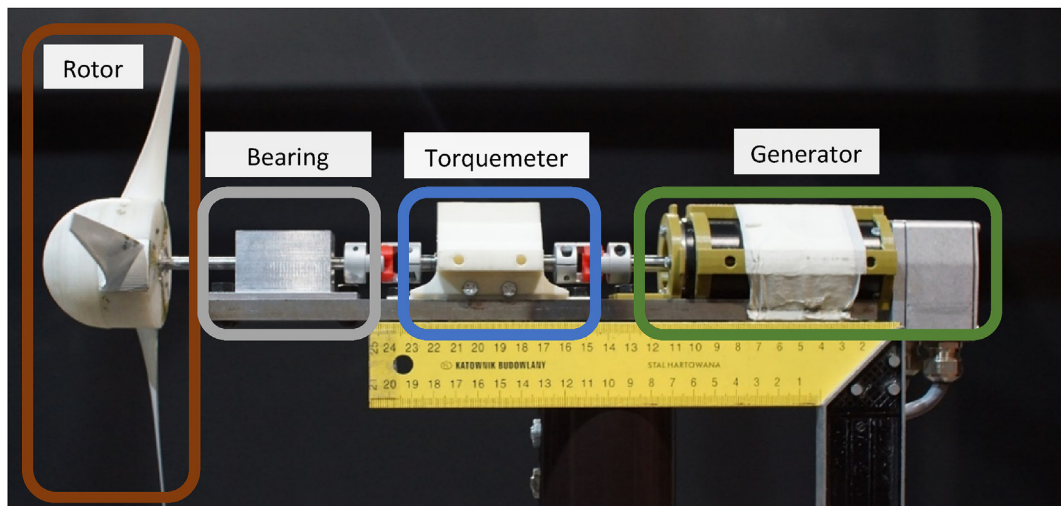
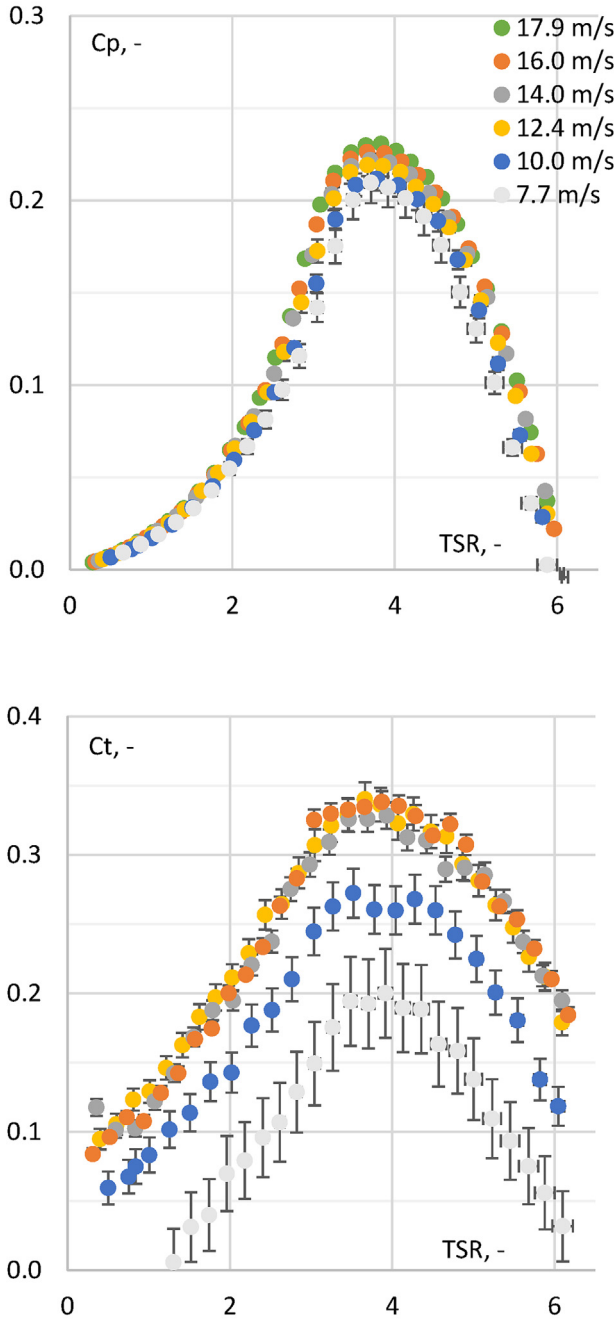


Fig. 5. T1 test setup overview (without covering).



**Fig. 6.**  $C_p$  and  $C_t$  vs TSR for different relative wind speeds  $V$ ; R1 open rotor (upwind). (For interpretation of the references to colour in this figure legend, the reader is referred to the Web version of this article.)

employment of the diffuser and the second rotor.

### 3.1. Small wind turbine operation in low-Re flows

The low Reynolds number observed at the SWT operation means that its blades will usually function in the transitory region between laminar and turbulent regimes (estimated to be around the Re order of magnitude  $10^5$ , see, e.g., Ref. [34]). The Reynolds number influence is most significant at low wind speeds and becomes less evident with an increasing wind speed. Fig. 6 presents wind turbine measurement results ( $C_p$  and  $C_t$  as functions of the

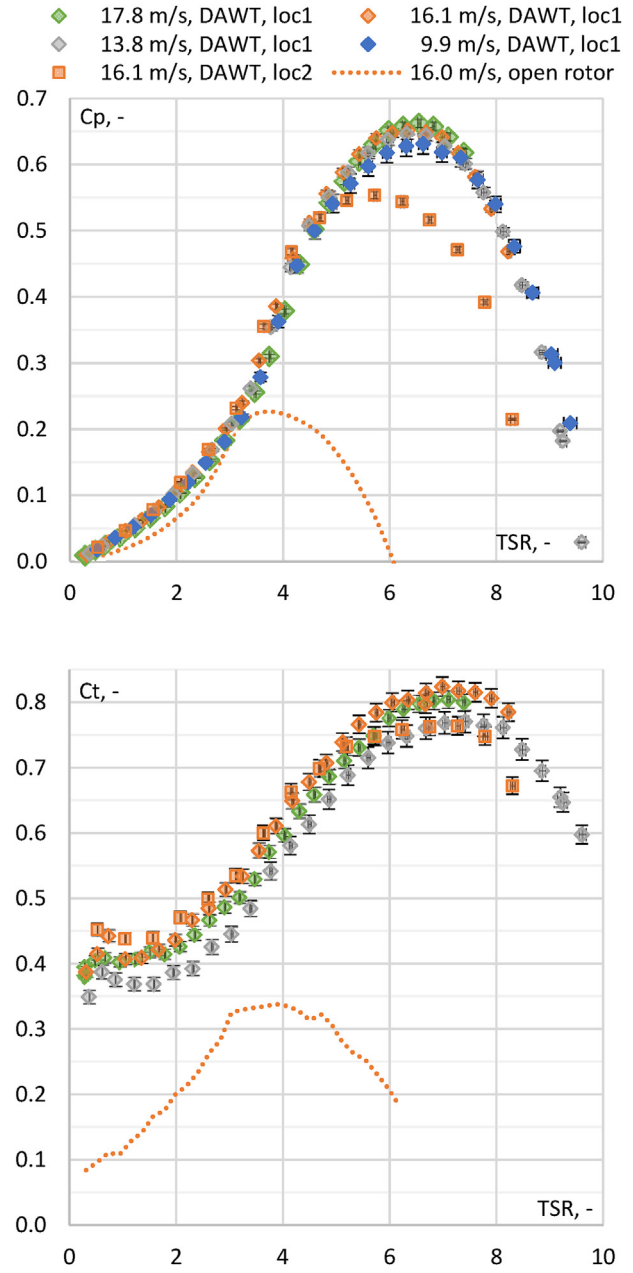


**Fig. 7.**  $C_p$  and  $C_t$  vs TSR for different relative wind speeds  $V$ ; R1 DAWT (downwind), R1 open rotor (upwind). (For interpretation of the references to colour in this figure legend, the reader is referred to the Web version of this article.)

TSR) for the wind speeds  $V$  in the range 8–18 m/s, with a step of approximately 2 m/s.

The characteristics for all wind speeds share a common region for the maximal  $C_p$  and  $C_t$  at approximately  $TSR = 3.5-4$ . All  $C_p$  curves remain very close at a low TSR (up to approximately  $TSR = 2$ ). With an increasing TSR, the curve traces start differing, yet this variation is inconsiderable. The difference in  $C_{pmax}$  between the reference velocities of 7.7 m/s and 17.9 m/s is equal to approximately 9%. As expected, the differences become less significant with an increase in the wind velocity. The characteristics captured for the reference wind speeds of 14.0 m/s, 16.0 m/s and 17.9 m/s share almost the same traces. The  $C_p$  values for 16.0 m/s and 17.9 m/s vary by no more than 2% along the entire TSR range under consideration. For all wind speeds, the predicted idle

rotational velocity is at about  $TSR = 6$ , but this value becomes higher as the relative wind speed rises. It is also visible that for the  $TSR$  above optimal, the  $C_p$  values remain globally higher for higher wind velocities. Under those conditions, the aerofoil operates at a low angle of attack, where the lift coefficient depreciates and the drag increases rapidly as the Reynolds number plummets (see, e.g., Ref. [35]). Consequently, at the same  $TSR$ , the resulting performance decreases with an increase in  $Re$ .

Concerning the values of  $C_t$ , differences are significantly more visible. The curves for the two lowest wind speeds (i.e., 7.7 m/s and 10.0 m/s) are located significantly lower than the rest of the curves. Since such significant differences are not reproduced in the  $C_p$  graph, this behaviour may be partially due to a low magnitude of the measured force and consequent limits of the measuring equipment, which is also confirmed by the prohibitively high level of uncertainty observed for this wind speeds. The characteristics for the reference wind speeds of 12.4 m/s, 14.0 m/s and 16.0 m/s share, once again, very similar traces, with differences up to approximately 5%. Note that the lack of the  $C_t(STR)$  curve for the wind speed 17.9 m/s comes from technical issues during data collection.

The above-mentioned observations permitted the reference velocity of about 16.0 m/s to be picked for further tests (except the cases when stated otherwise). On one hand, this velocity will contain the Reynolds number influence within acceptable limits, and, at the same time, the torque generated in the DAWT configuration will not surpass the generator-controller limits. The tests also show that – at extremely low  $Re$  flows – an increase in the wind speed through the rotor can dramatically improve the wind turbine performance, which is the principle of the DAWT operation.

### 3.2. Diffuser-Augmented Wind Turbine (DAWT)

Fig. 7 compares the performance of the DAWT and an open rotor wind turbine. The shrouding permitted the  $C_p$  to increase for the same wind velocity (16 m/s) by a factor of 2–3, which is not observed even for the examined twin-rotor systems (see Tables 2 and 3). This translates to an increase in the flow speed through the wind turbine rotor up to 40%. The obtained  $C_p$  increase is higher than that mentioned in literature: Kosasih and Tondelli [8] observed the maximal  $C_p$  rise by about 63% for a throat-equipped diffuser. In the current case, a significant amelioration is attributed to the fact that the rotor-diffuser assembly was optimised to operate together from the design stage. As a result, the ensemble is able to surpass the Betz limit for an open rotor. This is due to the fact that the local modification of pressure and velocity fields effectively violate the assumptions of the one-dimensional flow theory, as there is an additional contribution to the flow momentum due to the force exerted by the diffuser (see, e.g., Ref. [36]).

**Table 2**  
Maximal total  $C_p$  for the CROR.

Separation distance	Maximal $C_{ptot}$	Optimal $TSR1$	Optimal $TSR2$
a	0.251	3.66	3.16
b	0.251	3.66	3.08
c	0.256	3.64	2.94

**Table 3**  
Maximal total  $C_p$  for the CRSR.

Separation distance	Maximal $C_{ptot}$	Optimal $TSR1$	Optimal $TSR2$
a	0.582	5.32	4.52
b	0.515	5.16	3.82
c	0.579	5.12	3.44

Following a higher flow velocity through the rotor,  $\omega$  is also higher, achieving values of the order of magnitude of 10 000 rpm and more. At such high rotational velocities, the test operation becomes unstable and a blade fixation rupture is possible. Thus, the characteristics in this measurement campaign end mostly before reaching the idle operating conditions (at approximately  $TSR = 10$ ).

The wind turbine performance depends strongly on its position relative to the diffuser inlet. Location 1 in Fig. 7 denotes rotor placement directly at the diffuser narrowest cross-section. In location 2, the rotor is shifted upstream (by a distance of about 0.05 D) to permit accommodation of the downstream wind turbine in further tests. Consequently, in the latter case it operates at a lower local wind velocity (approximately 5%, as computed from the power difference), which in turn results in its lower power production (by about 15%).

As in the case of the open rotor, traces of the  $C_p$  characteristics tend to increase with an increasing wind velocity and, as previously, these differences become less significant as the wind speed increases. Overall, the differences between the 4 collected datasets are less significant than in the case of the open rotor configuration. This is also observed on the  $C_t$  graphs, where the differences are of the order of magnitude of 3% between 16.1 m/s and 17.8 m/s. It is also clearly seen that the results obtained for the open rotor are much lower than those for the ducted wind turbine. This mimics the situation observed previously for the open rotor examined at different wind speeds. It also shows that for the DAWT the price for increasing  $C_p$  is a drastic increase in axial loads (the maximal  $C_t$  higher by more than 130% at the wind speed of 16 m/s). The obtained results are coherent, for example, with the observations of Wang et al. [10], who saw an increase in the maximal tensile strains of the blade root by as much as 2–2.5 when a diffuser was applied. This is an important remark that needs to be considered when designing a DAWT rotor, as its blades have to withstand higher loads and stresses.

### 3.3. Counter-Rotating Open Rotor (CROR) wind turbine

In twin-rotor experiments, the two rotors face each other, as seen in Fig. 2. The upstream rotor remains at location 2 (see Section 3.2). The downstream rotor is placed at the distances 32 mm = 0.1D (diffuser inlet, case a), 96 mm = 0.3D (diffuser middle, case b), 200 mm = 0.625D (diffuser outlet, case c), respectively. The spherical cups topping the shafts were dismantled for the smallest separation distance. Fig. 8 compares the  $C_p$  characteristics for each wind turbine.  $C_{ptot}$  (the arithmetic sum of both power coefficients) and  $C_t$  for R1 are visible in Fig. 9.

The  $C_p1$  and  $C_p2$  coefficient distributions take a form of saddle-shaped surfaces. The  $C_p1$  surface shape follows roughly the trace of the  $C_p1$  curve without R2. The optimal  $TSR1$  remains in the vicinity of the same value (approximately 3.7) as for the open rotor.  $C_p1$  is globally lower than  $C_p$  of the open rotor, by approximately 20%–30% in the region of the optimal  $TSR$ . This is not a surprise, since the rotor separation distance is shorter than the rotor diameter. Thus, an interference of R2 and R1 cannot be neglected. This influence is best visible in case a, for which the saddle shape deepens as R2 approaches its optimal operating conditions. Contrarily, in case c the surface trace is almost constant along the entire  $TSR2$  range. In all, as the distance between the rotors increases, the attainable  $C_p1$  values increase as well, which once again can be attributed to a decreasing influence of R2 on R1.

As for  $C_p2$ , the distribution surface shapes remain very similar in all three locations, with a form of a relatively deep saddle. It is noticeable that, surprisingly, the  $C_p2$  values at CROR operation get lower with an increasing separation distance. As seen in the case of  $C_p1$ , a low separation distance promotes a strong interaction



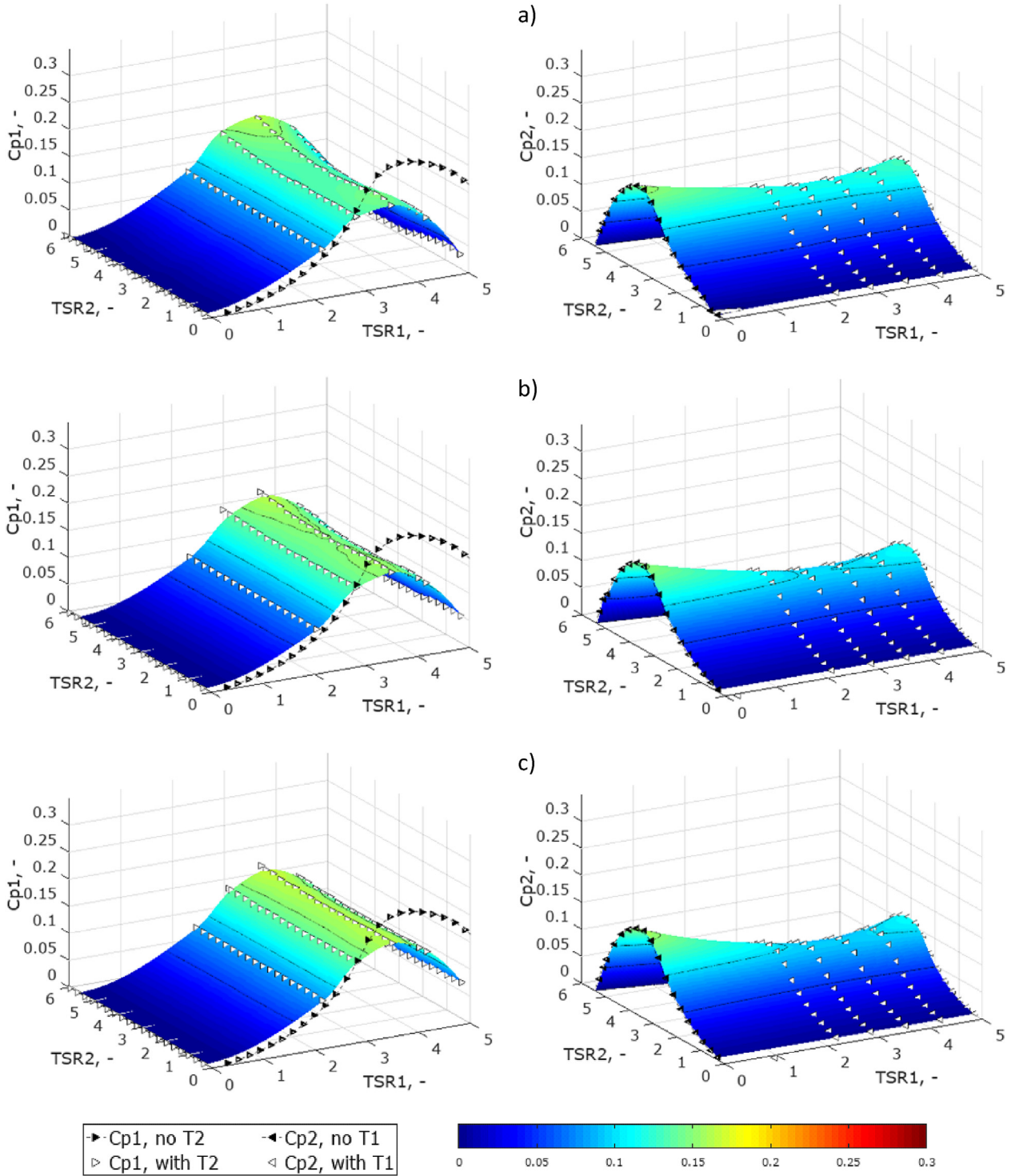


**Fig. 8.**  $C_p(TSR_1, TSR_2)$  for the upstream (R2, left) and downstream (R1, right) rotor operating in the CROR mode; rotor separation distance: 0.1D (a, top), 0.3D (b, middle), 0.625D (c, bottom); black points denote performance when only the rotor under consideration (either 1 or 2) is examined.

between the two rotors. Thus, the loads are more evenly distributed between the two rotors.

The R2 standalone characteristic curve attains lower values than that of R1 – this is because R2 measurements were performed with T1 in place. This characteristics attains higher maximal values with an increasing separation distance, since an influence of T1 decreases with an increasing distance.

Generally, the total power characteristics ( $C_{ptot}$  in Fig. 9) shows global maxima when the T1 wind turbine operates near the optimal point and T2 at a lower rotational velocity. The exact numerical values are seen in Table 2. In all three configurations, the CROR system achieves the maximal total  $C_p$  higher than that for a single wind turbine, by approximately 11%–13%. This observation proves that there is a potential in using CROR wind turbine systems, even

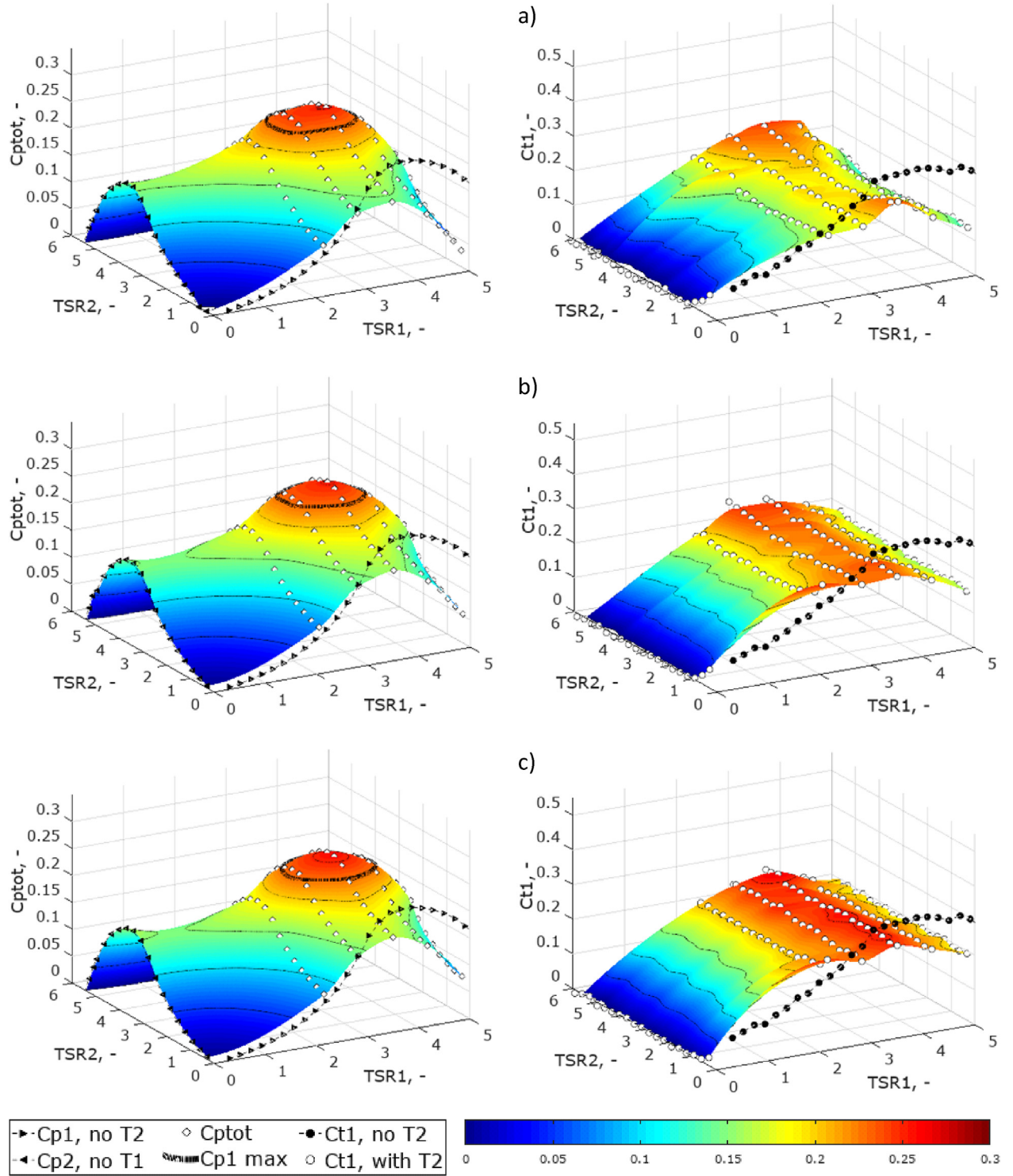


**Fig. 9.**  $C_{ptot}(TSR1, TSR2)$  (left) and  $C_{t1}(TSR1, TSR2)$  (right) for rotors operating in the CROR mode; rotor separation distance: 0.1D (a, top), 0.3D (b, middle), 0.625D (c, bottom); black points denote performance when only the rotor under consideration (either 1 or 2) is examined; thick black line ( $C_{p1}$  max) on the  $C_{ptot}$  graphs denotes  $C_p = 0.226$ , the maximal recorded  $C_p$  of the open rotor.

at small separation distances between rotor rotation planes (less than the rotor diameter). There is also room for further development: Kubo and Kanemoto [18] reported increasing the maximum  $C_{ptot}$  by as much as 35% by optimising the blades geometry (twist angles, chords, aerofoil), although this was done for two rotors of a different number of blades and diameters.

The operating region in which the CROR system presents better performance than a single open rotor spans between approximately  $TSR1$  between 2.6 and 4.2, and  $TSR2$  between 2.8 and 4.1. This means a relatively wide plateau of the preferable wind turbine operating conditions. It is also shifted towards lower  $TSR$  values than in the case of the standalone rotor operation. This can be

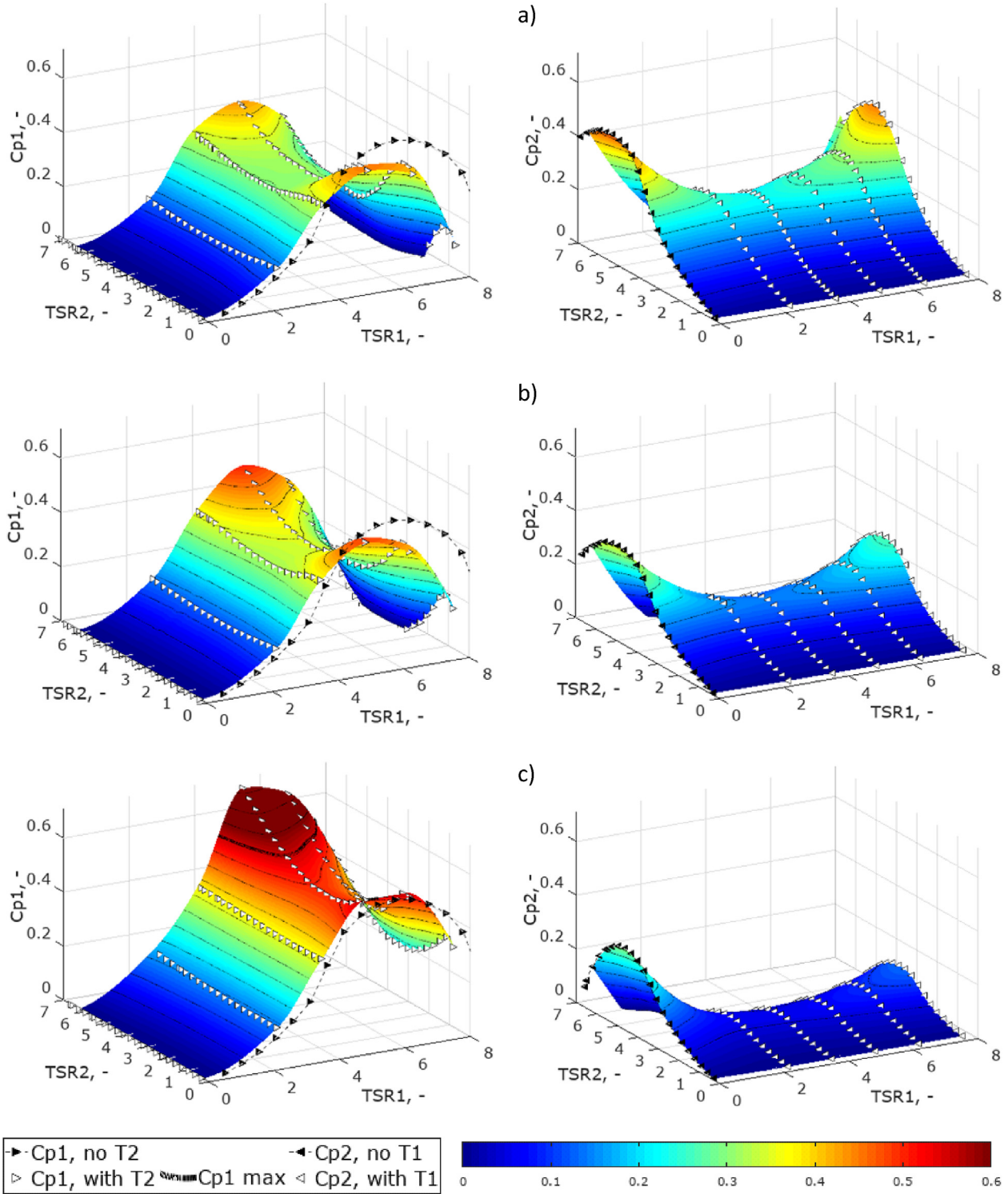


**Fig. 10.**  $C_p(TSR_1, TSR_2)$  for the upstream (R2, left) and downstream (R1, right) rotor operating in the CRSR mode; rotor separation distance: 0.1D (a, top), 0.3D (b, middle), 0.625D (c, bottom); black points denote performance when only the rotor under consideration (either 1 or 2) is examined; thick black line ( $C_{p1 \max}$ ) on the  $C_{p1}$  graph in case c denotes  $C_p = 0.554$ , the maximal recorded  $C_p$  for the DAWT.

translated into further advantages: easier rotational velocity control (the system may be less robust than in the case of a single open rotor), and lower mechanical efforts (lower rotational velocities and centrifugal forces). An interesting remark concerning the relative velocity of rotors can also be made. A change (increase or decrease) in rotational velocities of both rotors at the same time leads to a

quick and abrupt drop in the overall system performance. To change the relative rotational velocity, it is actually more efficiency-reasonable to maintain the TSR of one rotor at a near-to-optimal value and to change the rotational velocity of the other one.

As regards the  $C_{t1}$  parameter, similar observations can be forwarded as in the case of  $C_{p1}$ . An influence of R2 on R1 is the



strongest as the rotors approach each other (i.e., case a). As the separation distance increases, the saddle gets flatter in case b, to become almost completely uniform along the entire TSR2 span in case c. In total, the values of  $C_t$  are the highest for case c. This observation is consistent with the  $C_{p1}$  results, which in turn are

consistent with the one-dimensional flow theory. Compared to the standalone performance,  $C_{t1}$  in the CROR mode attains its maximum at the almost identical TSR1. The values for CROR are, however, lower than for the single rotor operation, similarly to those observed in the case of  $C_{p1}$ . This enables to formulate a

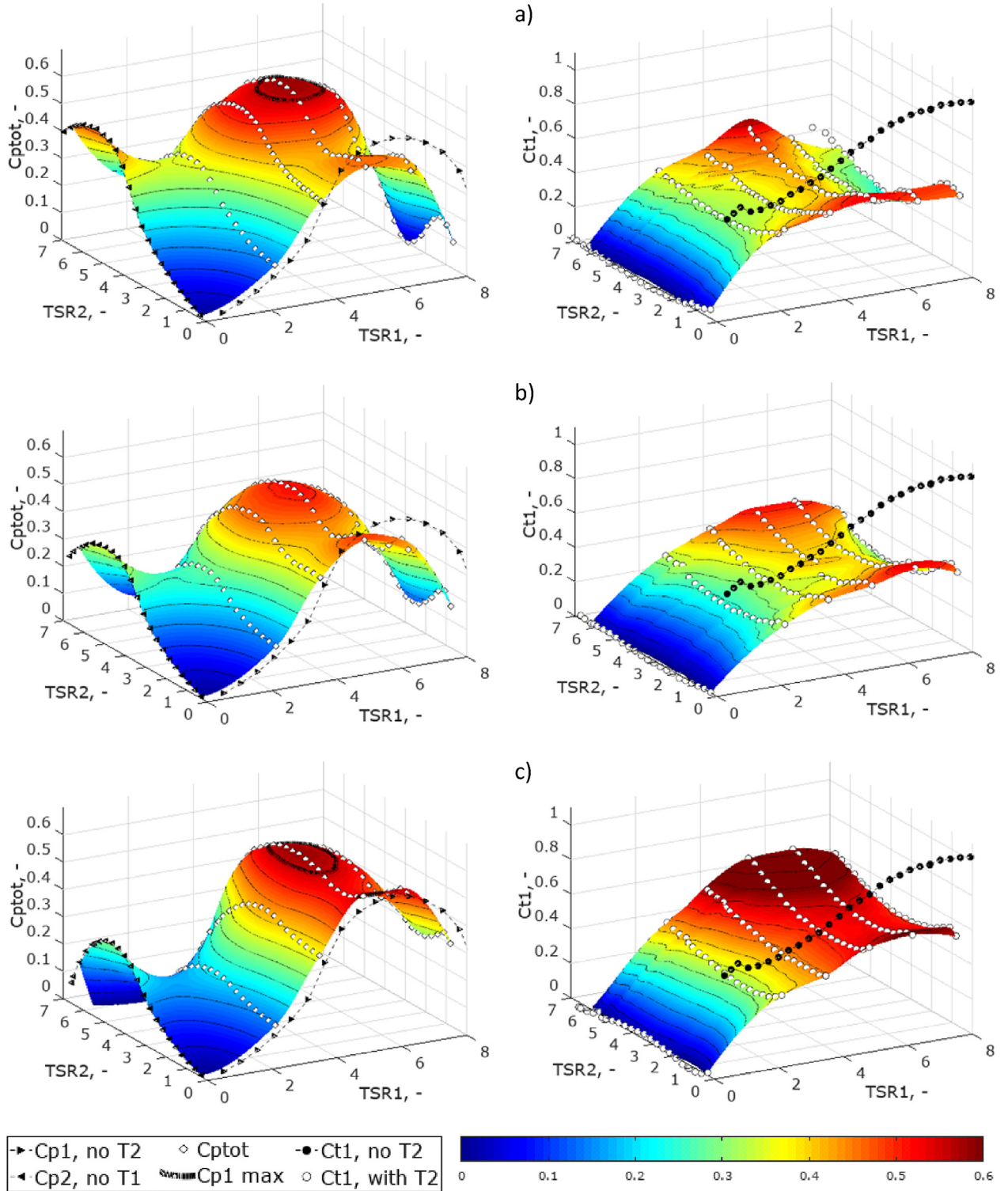


**Fig. 11.**  $C_{ptot}(TSR_1, TSR_2)$  (left) and  $C_{t1}(TSR_1, TSR_2)$  (right) for rotors operating in the CROR mode; rotor separation distance: 0.1D (a, top), 0.3D (b, middle), 0.625D (c, bottom); black points denote performance when only the rotor under consideration (either 1 or 2) is examined; thick black line ( $C_{p1}$  max) on the  $C_{ptot}$  graphs denotes  $C_p = 0.554$ , the maximal recorded  $C_p$  for the DAWT.



hypothesis that the stresses in blades were decreased with a distribution of loads on the two rotors.

### 3.4. Counter-Rotating Shrouded Rotor (CRSR) wind turbine

The  $C_p$  characteristics for both wind turbines (Fig. 10) are of a saddle shape once again, as in the case of the CROR. An interaction of these two machines is, however, both stronger and steeper than previously. Additionally, an influence of  $R_2$  on  $R_1$  becomes stronger as the separation distance rises, especially at  $TSR_1$  close to optimal. As the separation distance rises, the range of  $TSR_2$  in which  $R_2$  operates as a turbine is getting smaller: in case c,  $C_{p2}$  becomes negative at  $TSR_2 > 4-5$ . The negative power means in this context that the energy is transmitted from the rotor to the fluid, signifying that it effectively operates as a fan. This means that immediately upstream of  $R_2$ , the pressure is decreased, contributing to the deficit existing already inside the diffuser and augmenting additionally the flow rate through  $R_1$ . Hence, a significant increase in  $C_{p1}$  values at high  $TSR_2$  in cases b and c is observed. However, this comes at the expense of a high power demand of  $R_2$ , which results in low net total power (and, thus,  $C_{ptot}$ , cf. Fig. 11). The study and development of such a “turbofan” system might be of interest for future works. However, at this moment a possibility of positive energy balance of such a system is unlikely. Also, the diffuser outlet is a region of high pressure gradients and strong separations. Placement of the rotor in this region promotes its unstable operation, increasing stresses and fatigue wear, as well as vibrations of the diffuser and both the rotors.

Generally,  $C_{p1}$  values tend to increase along with a separation distance between the two rotors. This is an adverse information, in that the highest velocity augmentation in the diffuser occurs at its inlet, thus an interest in placing both the rotors in that region. In the meantime,  $C_{p2}$  values are the highest at a low separation distance. As the distance increases, the operation range of  $T_2$  gets narrower and the power outcome becomes abysmal. In case a, the maximal value of  $C_{p2}$  (at  $TSR_1 = 0$ ) is about 0.476, whereas in case c, it is equal to 0.302. In case a, maximal  $C_{p2}$  values are higher by as much as 5 times than those for case c. Consequently,  $C_{ptot}$  (Fig. 11) attains its high values in cases a (due to high  $C_{p2}$ ) and c (thanks to high  $C_{p1}$ ). These values surpass the maximal  $C_{p1}$  for the single-rotor DAWT, i.e., 0.554.

It can be also seen that in case c, when  $TSR_2$  is very low,  $C_{p2}$  attains almost the same values as for the single-rotor DAWT. This means that with the highest separation distance between the two rotors and at low  $TSR_2$ , an influence of  $T_2$  on  $T_1$  is marginal.

Similarly as in the case of the CROR, high overall performance of the CRSR is ensured at a plateau around optimal functioning conditions (see Table 3). This plateau is of a comparable size for both open and shrouded rotors (notice different scales in both cases). It is, however, very clear that in order to maximise  $C_{ptot}$ , it is particularly important to maintain  $TSR_1$  near the optimal value. This is especially visible in case c, for which even a small decrease in  $TSR_1$  below the value of 4 results in a dramatic loss of power outcome.

Considering the distribution of  $C_{t1}$  values, the saddle shape mimics that observed for  $C_{p1}$ . The surfaces become steeper as the separation distance increases. The latter also results in attaining globally higher  $C_{t1}$  values, although they are still significantly lower than the ones for the single-rotor DAWT. Local maxima of the characteristics fall at approximately the same  $TSR$  values as the  $C_{p1}$  maxima.

## 4. Summary and conclusions

This paper summarizes and discusses the IMP TUL experimental

investigations concerning various aspects of the SWT operation. The main focus has been placed on an increase in the wind turbine system efficiency through diffuser augmentation (DAWT) and an addition of the second rotor (CROR). The study concludes with a complex examination of the machine combining both the above-mentioned solutions (CRSR).

The experimental results allow one to formulate the following observations and conclusions:

- The maximal power coefficient of the wind turbine decreases significantly along with the wind reference speed. This is due to relatively low values of the Reynolds number (of the order of  $10^5$ , as determined on the basis of the rotor diameter), which is a significant obstacle in the investigations and aerodynamic optimisation of small wind turbines. The study permitted to quantify this dependency;
- After an application of shrouding, an approximately twofold increase in the upstream wind turbine power coefficient has been observed at the same wind speed. This is a very significant amelioration, although it must be underlined that the tested rotor-diffuser system has been aerodynamically optimised. An increase in the  $TSR$  corresponding to the maximal  $C_p$  value (from 4.5 to 6) and an increase in the axial force coefficient have been also observed. Increased blade loading and internal stresses have to be taken into account during the DAWT design process;
- The use of the second rotor has allowed one to increase the total power coefficient by about 11–13% in the case of the unshrouded turbine and about 4–5% for the shrouded one. The latter, relatively poor result, is once again attributed to the fact that the diffuser-turbine arrangement has been optimised to operate together as mentioned above, favouring the single-rotor solution;
- Thanks to the use of the two-rotor system, it has been possible to reduce the thrust coefficient of the upstream turbine and to decrease the optimal  $TSR$  (by about 20% for the upstream rotor and 33% for the downstream one, respectively). This may also lead to a better distribution of stresses in the blades of both the rotors;
- Due to the presence of the second rotor, the  $TSR$  range in which the system worked with  $C_p$  close to the maximum has been also widened;
- The maximal cumulative  $C_p$  is strongly dependent on the mutual position of the rotors. Notably, as the downstream rotor approaches the diffuser outlet, the range of  $TSR$  for which it operates as a turbine (i.e., receives energy from the flow) decreases significantly.

The obtained and presented results show a potential for increasing the wind turbine performance for shrouded rotors, counter rotating rotors and CRSR systems. A further analysis of these systems employing more extensive flow measurements or numerical simulation methods is to be performed.

## Conflicts of interest

The authors declare no conflict of interest.

## Funding

This research was funded within the Polish Ministry of Science and Higher Education programme “Diamond Grant” (DI2013 011843).

## References

- [1] Igra O. Research and development for shrouded wind turbines. *Energy Conversion and Management* 1981;21(1):13–48.
- [2] Gilbert BM, Foreman KL. Experiments with a diffuser-augmented model wind turbine. *Journal Energy Resources Technology* 1983;105:46–53.
- [3] Abe K-I, Ohya Y. An investigation of flow fields around flanged diffusers using CFD. *J Wind Engineering and Industrial Aerodynamics* 2004;92:315–30.
- [4] Al-Sulaiman FA, Yilbas BS. Thermoeconomic analysis of shrouded wind turbines. *Energy Conversion and Management* 2015;96:599–604.
- [5] Commission IE. IEC 61400-2: wind turbines - Part 2. Small wind turbines; 2013.
- [6] Krog L, Sperling K, Lund H. Barriers and recommendations to innovative ownership models for wind power. *Energies* 2018;11:2602.
- [7] Nagai M, Irabu K. Momentum theory of diffuser augmented wind turbine (in Japanese). *Transactions of the Japan Society of Mechanical Engineers Series B* 1987;53(489):1543–7.
- [8] Kosasih B, Tondelli A. Experimental study of shrouded micro-wind turbine. *Procedia Engineering* 2012;49:92–8.
- [9] Abe K-I, Nishida M, Sakurai A, Ohya Y, Kihara H, Wada E, Sato K. Experimental and numerical investigations of flow fields behind a small wind turbine with a flanged diffuser. *J Wind Engineering and Industrial Aerodynamics* 2005;93: 951–70.
- [10] Wang W-X, Matsubara T, Hu J, Odahara S, Nagai T, Karasutani T, Ohya Y. Experimental investigation into the influence of the flanged diffuser on the dynamic behavior of CFRP blade of a shrouded wind turbine. *Renewable Energy* 2015;78:386–97.
- [11] Grönman A, Backman J, Hansen-Haug M, Laaksonen M, Alkki M, Aura P. Experimental and numerical analysis of vaned wind turbine performance and flow phenomena. *Energy* 2018;159:827–41.
- [12] Olasek K, Karczewski M, Lipian M, Wiklak P, Józwick K. Wind tunnel experimental investigations of a diffuser augmented wind turbine model. *Int J Numerical Methods for Heat & Fluid Flow* 2016;26(7).
- [13] Curtis CG. Elastic-fluid turbine. New York: United States of America Patent; 1 September 1896, 566969.
- [14] Dou B, Guala M, Lei L, Zeng P. Experimental investigation of the performance and wake effect of a small-scale wind turbine in a wind tunnel. *Energy* 2019;166:819–33.
- [15] Appa K. Counter-rotating wind turbine system. Lake Forest: " Appa Technology Initiatives; 2002.
- [16] Jung SN, No T-S, Tyu K-W. Aerodynamic performance prediction of a 30 kW counter-rotating wind turbine system. *J Renewable Energy* 2005;30:631–44.
- [17] Kanemoto T, Galal AM. Development of intelligent wind turbine generator with tandem wind rotors and double rotational armatures (1st report, superior operation of tandem wind rotors). *JSME International Journal Series B Fluids and Thermal Engineering* 2006;49:450–7.
- [18] Kubo K, Kanemoto T. Development of intelligent wind turbine generator with tandem wind rotors and double rotational armatures (2nd report, Characteristics of tandem WR). *J Fluid Science and Technology* 2008;3(3):370–8.
- [19] Kubo K, Hano Y, Mitarai H, Hirano K, Kanemoto T, Galal AM. Intelligent wind turbine unit with tandem rotors (discussion of prototype performances in field tests). *Current Applied Physics* 2010;10:326–31.
- [20] Gipe P. Wind energy for the rest of Us: a Comprehensive Guide to wind power and how to Use it. Bakersfield, CA: wind-works.org; 2016.
- [21] Göltenbott U, Ohya Y, Yoshida S, Jamieson P. Aerodynamic interaction of diffuser augmented wind turbines in multi-rotor systems. *Renewable Energy* 2017;112:25–34.
- [22] Burton T, Jenkins N, Sharpe D, Bossanyi E. *Wind energy Handbook*. second ed. West Sussex: John Wiley & Sons; 2011.
- [23] Hansen MOL. *Aerodynamics of wind turbines*. second ed. London: Earthscan; 2008.
- [24] Newman B. Multiple actuator-disc theory for wind turbines. *Journal of Wind Engineering and Industrial Aerodynamics* 1986;24:215–25.
- [25] Bartl J, Saetran L. Blind test comparison of the performance and wake flow between two in-line wind turbines exposed to different turbulent inflow conditions. *Wind Energy Science* 2017;2:55–76.
- [26] Kądrowski D, Kulak M, Lipian M, Stepień M, Baszczynski P, Zawadzki K, Karczewski M. Challenging low Reynolds - SWT blade aerodynamics. *MATEC Web of Conferences* 2018;234.
- [27] Barlow JB, Rae Jr WH, Pope A. *Low-speed wind tunnel testing*. third ed. New York, NY: John Wiley&Sons, Inc.; 1999.
- [28] Buck AL. New equations for computing vapor pressure and enhancement factor. *J Applied Meteorology* 1981;20:1527–32.
- [29] Porocznicki J, Prywer J. Aerodynamic tunnel for the investigations of cascade blades. *Ciepłne Maszyny Przepływowe* 1981;89(389):217–26.
- [30] Kulak M, Karczewski M, Olasek K, Jankowski K. Numerical simulations and experimental study of wind tunnel turbulence intensity reduction. *Ciepłne Maszyny Przepływowe - Turbomachinery* 2007;132:14.
- [31] Józwick K, Karczewski M, Lipian M, Olasek K, Pycio P, Wiklak P. "Experimental stand for wind turbine power measurements (No. Arch. 1851) – STOW project report. Lodz, Poland: " IMP TUL; October 2015.
- [32] Kulak M, Karczewski M, Olasek K, Józwick K. CFD analysis of Diffuser Augmented Wind Turbine model for wind tunnel investigation. In: *Industrial Electronics Society, IECON 2016. 42nd. Florence: Annual Conference of the IEEE; 2016.*
- [33] Lipian M, Kulak M, Stepień M. Fast track integration of computational methods with experiments in small wind turbine development. *Energies* 2019;12(9):1625. 29 4.
- [34] Giguère P, Selig MS. New airfoils for small horizontal Axis wind turbines. *Journal of Solar Energy Engineering* 1998;120:108–14.
- [35] Lyon CA, Broeren AP, Giguere P, Gopalathnam A, Selig MS. In: *Summary of low-speed airfoil data*, vol. 3. Virginia Beach: SoarTech Publications; 1997.
- [36] Aranake AC, Lakshminarayan VK. Assessment of low-order theories for analysis and design of shrouded wind turbines using CFD. *Journal of Physics: Conference Series* 2014;524.